

Surface-enhanced Raman scattering on periodic metal nanotips with tunable sharpness

This article has been downloaded from IOPscience. Please scroll down to see the full text article.

2009 Nanotechnology 20 225303

(<http://iopscience.iop.org/0957-4484/20/22/225303>)

The Table of Contents and more related content is available

Download details:

IP Address: 131.252.177.86

The article was downloaded on 12/05/2009 at 21:20

Please note that terms and conditions apply.

Surface-enhanced Raman scattering on periodic metal nanotips with tunable sharpness

Nicholas C Linn¹, Chih-Hung Sun¹, Ajay Arya¹, Peng Jiang^{1,3} and Bin Jiang²

¹ Department of Chemical Engineering, University of Florida, Gainesville, FL 32611, USA

² Department of Mathematics and Statistics, Portland State University, Portland, OR 97201, USA

E-mail: pjiang@che.ufl.edu

Received 13 January 2009, in final form 3 April 2009

Published 12 May 2009

Online at stacks.iop.org/Nano/20/225303

Abstract

This paper reports on a scalable bottom-up technology for producing periodic gold nanotips with tunable sharpness as surface-enhanced Raman scattering (SERS) substrates. Inverted silicon pyramidal pits, which are templated from non-close-packed colloidal crystals prepared by a spin-coating technology, are used as structural templates to replicate arrays of polymer nanopyramids with nanoscale sharp tips. The deposition of a thin layer of gold on the polymer nanopyramids leads to the formation of SERS-active substrates with a high enhancement factor (up to 10^8). The thickness of the deposited metal determines the sharpness of the nanotips and the resulting Raman enhancement factor. Finite-element electromagnetic modeling shows that the nanotips can significantly enhance the local electromagnetic field and the sharpness of nanotips greatly affects the SERS enhancement.

(Some figures in this article are in colour only in the electronic version)

1. Introduction

Surface-enhanced Raman scattering (SERS) is of considerable technological importance and great scientific interest in developing ultra-sensitive chemical and biological sensors as well as fundamental understanding of spatial confinement and enhancement of electromagnetic field enabled by plasmonic metal nanostructures [1–12]. Stochastically aggregated colloidal nanoparticles and electrochemically roughened metal surfaces have been extensively exploited as SERS substrates [5, 13–21]. However, the poor reproducibility of SERS enhancement, which is caused by the random distribution of electromagnetic ‘hot spots’, has greatly impeded the practical applications of these substrates. Periodic metal nanostructures have therefore been developed to resolve the reproducibility issue [22–27]. Sophisticated nanolithography technologies (e.g., electron-beam lithography and focused ion-beam) can reproducibly

generate arbitrary plasmonic nanostructures with sub-50 nm resolution [2, 8, 28]. Nevertheless, attaining high throughput and large-area fabrication continues to be a major challenge with these top-down approaches.

Bottom-up colloidal self-assembly and subsequent templating nanofabrication provide a much simpler, faster, and inexpensive alternative to nanolithography for producing structured SERS substrates [22–27]. Nanosphere lithography (NSL) uses monolayer or double-layer colloidal crystals as sacrificial deposition masks to create two-dimensional (2D) ordered metal nanoparticles in the voids of the nanospheres [25, 29]. SERS enhancement factor of $\sim 9.0 \times 10^7$ has been demonstrated for arrays of silver nanoparticles produced by NSL [25]. Macroporous multilayer films and sculpted metals with hexagonal arrays of sphere segment nanovoids have been fabricated by completely filling the interstitials of self-assembled colloidal crystals with coinage metals or metal nanoparticles [23, 26]. High and reproducible SERS enhancement (on the order of 10^7) has been observed for these structured substrates. Isolated colloidal particles can

³ Author to whom any correspondence should be addressed.

also be used as sacrificial templates to generate crescent moon-like gold nanoparticles with sub-10 nm sharp edges [30, 31]. The edges can efficiently concentrate local electromagnetic field, resulting in a great enhancement of the Raman scattering intensity. Although the current bottom-up approaches are favorable for low-volume, laboratory-scale production of SERS-active substrates, the low throughput and incompatibility with standard microfabrication greatly impede the scaling-up and cost efficiency of these unconventional technologies. In addition, the colloidal templates are destroyed during the fabrication process, further limiting the throughput and the reproducible production of SERS substrates with the similar structural parameters.

We have recently developed a scalable and microfabrication-compatible bottom-up technology that enables the fabrication of periodic gold nanopylramids with nanoscale sharp tips and wafer-scale area (larger than 4 inch in diameter) [32, 33]. In this approach, arrays of inverted silicon pyramidal pits which are templated from monolayer colloidal crystals prepared by a simple spin-coating technology are employed as reusable molds to replicate gold nanopylramids. The major drawback of the technology is the high material cost as a 500 nm thick gold layer needs to be deposited to create the nanopylramid arrays. Moreover, due to the relatively weak mechanical strength of gold and the adhesion of gold on the sidewalls of the inverted silicon pits, a large number of the resulting gold nanopylramids are broken when peeling off the gold film from the silicon template. The broken nanopylramids greatly affect the concentration of electromagnetic field in the vicinity of the nanotips, resulting in low SERS enhancement ($\sim 7 \times 10^5$), which is orders of magnitude lower than those of other SERS substrates created by colloidal templating approaches [23, 25]. Here we demonstrate that much higher enhancement factor (up to 10^8) can be achieved by using gold-covered polymer nanopylramid arrays as SERS-active substrates. A much thinner gold layer (10–30 nm thick) is sufficient to generate the high SERS enhancement. The sharpness of the templated nanopylramids can also be tuned by controlling the thickness of the deposited gold. Finite-element electromagnetic modeling has been employed to simulate the SERS enhancement surrounding arrays of gold-covered polymer nanopylramids with different tip sharpness.

2. Experimental details

2.1. Materials and substrates

All solvents and chemicals are of reagent quality and are used without further purification. Technical-grade KOH flakes and anhydrous 2-propanol are purchased from Fisher Chemicals and Sigma-Aldrich, respectively. Ultrapure water ($18.2 \text{ M}\Omega \text{ cm}^{-1}$) is used directly from a Barnstead water system. Benzenethiol (>98% purity) is purchased from Sigma-Aldrich. Monodispersed silica colloids with 320 nm diameter and less than 5% diameter variation are synthesized by the Stöber method [34]. Ethoxylated trimethylolpropane triacrylate (ETPTA) monomer is obtained from Sartomer (Exton, PA). The photoinitiator, Darocur 1173 (2-hydroxy-2-methyl-1-phenyl-1-propanone), is provided by Ciba Specialty

Chemicals. (3-acryloxypropyl)trichlorosilane (APTCS) and octadecyltriethoxysilane (OTE) are purchased from Gelest and Alfa Aesar, respectively. Silicon wafers (test grade, n type, (100)) are obtained from Wafernet and are primed by swabbing APTCS on the wafer surfaces using cleanroom Q-tips (Fisher), rinsed and wiped with 200-proof ethanol three times, spin-coated with a 200-proof ethanol rinse at 3000 rpm for 1 min, and baked on a hot plate at 110 °C for 2 min. The same APTCS-priming process is also used to prime glass slides (Corning 2947).

2.2. Instrumentation

Scanning electron microscopy is carried out on a JEOL 6335F FEG-SEM. A thin layer of gold is sputtered onto the samples prior to imaging. Atomic force microscope (AFM) is conducted on a Digital Instruments Dimension 3100 unit. A WS-400B-6NPP-Lite Spin Processor (Laurell) is used to spin-coat colloidal suspensions. The polymerization of ETPTA monomer is carried out on a pulsed UV curing system (RC 742, Xenon). Oxygen plasma etch is performed on a Unaxis Shuttlelock RIE/ICP reactive-ion etcher. A Denton DV-502A electron-beam evaporator and a Kurt J Lesker CMS-18 multitarget sputter are used to deposit metals. Raman spectra are measured with a Renishaw inVia confocal Raman microscope.

2.3. Preparation of gold-covered polymer nanopylramid arrays

The fabrication of wafer-scale, monolayer, non-close-packed silica colloidal crystal-ETPTA nanocomposites on (100) silicon wafers is performed by following the established spin-coating procedures [35, 36]. The ETPTA matrix is removed by oxygen plasma etch operated at 40 mTorr pressure, 40 sccm flow rate, and 100 W for 2 min. The released silica particles are used as shadow masks during the electron-beam deposition of a 30 nm thick chromium layer. Chromium nanohole arrays are resulted after removing the templating silica particles by rubbing the wafer with a cleanroom Q-tip under flowing water. The wafer is then wet etched at 60 °C for 210 s in a freshly prepared solution containing 62.5 g of KOH, 50 ml of anhydrous 2-propanol, and 200 ml of ultrapure water to generate inverted pyramids in silicon. After dissolving the chromium layer in CR-7 etchant (Transene), the silicon wafer is immersed in the hydrolysis solution of octadecyltriethoxysilane (0.02 M), H₂O (0.28 M), and HCl (0.0066 M) in tetrahydrofuran (THF) for 30 min. The OTE-modified silicon wafer is then put on top of ETPTA monomer supported by an APTCS-primed glass slide with spacers (double-stick tape, thickness of ~ 0.1 mm) in between. Polymer nanopylramid arrays can then be made by curing ETPTA monomer and peeling off the silicon template. A thin layer of gold with various thicknesses can finally be deposited by sputtering to generate SERS-active substrates.

2.4. Raman spectra measurements

The gold-covered polymer nanopylramid arrays are immersed in a 5 mM solution of benzenethiol in 200-proof ethanol for

45 min and then rinsed in 25 ml of 200-proof ethanol for several minutes. The samples are finally dried in air for 20 min. A flat gold film deposited on a glass slide by the same sputtering process is used as the control sample for Raman spectra measurements. Raman spectra are obtained using a 785 nm diode laser at 4.8 mW with integration time of 10 s and a $40 \mu\text{m}^2$ spot size.

2.5. Electromagnetic modeling of Raman enhancement

In the finite-element method (FEM) model [37], we suppose that the gold nanopyramid array is placed horizontally so that the interface between the substrate and the medium (air) is parallel to the xz plane while the nanopyramids are along the y axis. For clarification of our approach, let us consider the transverse magnetic field (TE and hybrid modes can be handled similarly) so that the incident electric and magnetic fields go along x and z directions and can be expressed as:

$$E_{\text{inc},x} = E_0 e^{-j\frac{2\pi}{\lambda}y} \hat{x}, \quad H_{\text{inc},z} = H_0 e^{-j\frac{2\pi}{\lambda}y} \hat{z}$$

where E_0 and H_0 are the incident electric and magnetic field amplitudes, and λ is the wavelength of the incident light. The total electromagnetic fields $E = E_{\text{inc}} + E_{\text{scatter}}$ and $H = H_{\text{inc}} + H_{\text{scatter}}$ should satisfy Maxwell's equations within both medium and scatter (gold) domains:

$$\begin{aligned} \nabla \times (\nabla \times E) - \omega^2 \varepsilon \mu E &= 0 \\ \nabla \times (\nabla \times H) - \omega^2 \varepsilon \mu H &= 0 \end{aligned} \quad (1)$$

where ε and μ are domain-dependent permittivity and permeability, $\omega = \frac{2\pi}{\lambda}$ is the light frequency, $E = (E_x, E_y, 0)$ and $H = (0, 0, H_z)$. Continuity of tangential components of E and H across the interface between air and gold leads to the following boundary conditions with n as the interfacial normal vector:

$$\begin{aligned} (E_1 - E_2) \times n &= 0 \\ (H_1 - H_2) \times n &= 0. \end{aligned} \quad (2)$$

We employed FEM under Comsol Multi-physics environment to obtain numerical solutions of the equations (1) and (2) for each substance (air and gold). It should be noted that Comsol provides cutting-edge numerical algorithms, has convenient adaptive meshing techniques, and also allow users to establish their own modules with specific differential equations and boundary conditions to solve user-specific questions. In order to obtain high-resolution numerical solutions, the computational domain needs to be bounded and the boundary conditions should be well defined. To this end, we utilized the 'perfect matched layers' (PML) boundary approach for the simulation [38]. We artificially constructed ten boundary layers around the medium and the scatter domains. The electronic and magnetic conductivity of each boundary layer can be set artificially so that little or no electromagnetic radiation will be reflected back into the domain of scatter. To simulate electromagnetic fields in the newly augmented domains, we solved Maxwell equation (1) in all the sub-domains. The boundary condition (2) still holds for all internal interfaces. As to the outer boundaries of the PML

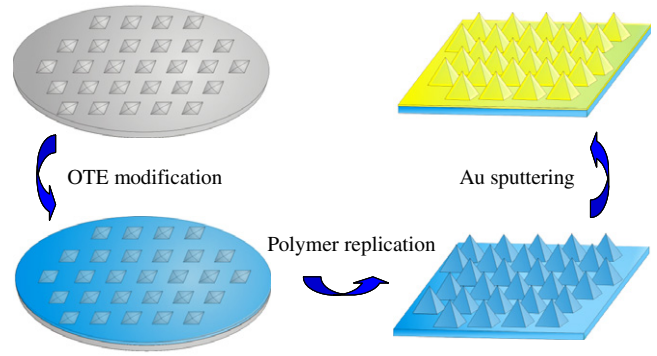


Figure 1. Schematic outline of the templating procedures for fabricating arrays of gold-covered polymer nanopyramids by using inverted silicon pyramidal pits as template.

layers, a low-reflection boundary condition (3) is provided to minimize residual reflection and attenuate the wave quickly within the layers:

$$n \times (\nabla \times H_z) - j\omega H_z = 0. \quad (3)$$

After solving Maxwell equation (1) together with boundary conditions (2) and (3), the two-dimensional electric field can be used to calculate the Raman enhancement as $G(x, y) = \log(|\frac{E(x,y)}{E_0}|^4)$, where $E(x, y)$ is the electric field amplitude at location (x, y) [37, 39]. The maximum value of the Raman enhancement can be obtained over the medium domain.

3. Results and discussion

The schematic outline of the templating procedures for fabricating arrays of gold-covered polymer nanopyramids with nanoscale sharp tips is shown in figure 1. Inverted pyramidal pits in (100) silicon wafers are first templated from periodic chromium nanoholes which are replica of hexagonally ordered silica colloidal monolayers prepared by a scalable spin-coating technology [35, 36]. The surface of the templated silicon pits is then functionalized by octadecyltriethoxysilane (OTE) by the well-established silane-coupling reactions [40]. The modified silicon substrates can then be used as structural templates to replicate polymer nanopyramid arrays by photopolymerizing ethoxylated trimethylolpropane triacrylate (ETPTA) monomers in the inverted pits. The low surface energy of the OTE coating reduces the adhesion of the cured polymer, facilitating the easy peeling of the polymer nanopyramid arrays from the silicon template. The glass slide, which is used to support the resulting polymer nanopyramids, can be primed by (3-acryloxypropyl)trichlorosilane to induce the formation of covalent bonds between polymer and glass to further enhance the peeling simplicity [35]. Multiple polymer replicas with almost identical structural parameters can thus be replicated from a single silicon template. A thin layer of gold can finally be sputtered onto the polymer nanopyramids to create the SERS-active substrates.

Figure 2 shows the top-view scanning electron microscope (SEM) image of an array of inverted silicon pyramidal pits

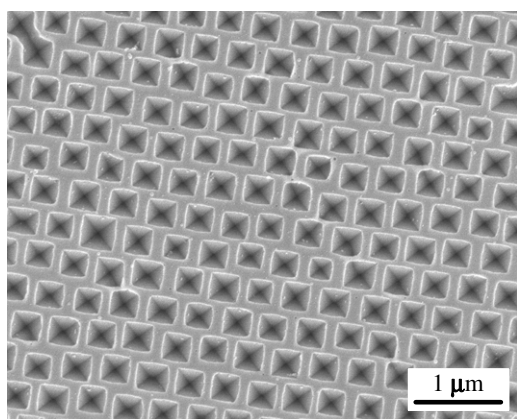


Figure 2. Top-view SEM image of an array of inverted silicon pyramidal pits templated from a spin-coated colloidal crystal consisting of 320 nm silica spheres.

created by KOH wet etch at 60°C for 210 s using a spin-coated colloidal crystal consisting of 320 nm silica spheres as template. The pyramidal pits have well defined square bases and the orthogonal crosses at the centers of the pits confirm the inverted pyramidal structures. The base length of the pyramids (~360 nm) is larger than that of the templating silica spheres due to the undercutting of the silicon substrate underneath the chromium nanoholes. The long-range hexagonal ordering of the inverted pits is also clearly evident from the SEM image and is further confirmed by the iridescent colors of the patterned silicon wafer that are caused by the diffraction of visible light by the periodic pits. The common defects include grain boundaries between single-crystalline domains (typical size of several hundred microns) and adjoining pits (see the pits in the upper left corner of figure 2), though these defects do not affect the sharpness of the vertex of the inverted pyramidal pits. As demonstrated in our previous work, the base length of the templated pits can be easily tuned by controlling the anisotropic KOH wet etch conditions (e.g., reaction temperature and duration) [32]. The depth of the inverted pits is solely determined by the base length as the wet etched pyramids have characteristic 54.7° sidewalls [41]. The inter-pit distance is identical to the inter-particle distance of the original silica colloidal crystal that equals to $\sqrt{2}D$, where D is the diameter of the templating silica spheres [35].

To prevent the breaking of the sharp nanotips during peeling off the polymer nanopyramids from the silicon template, the sidewalls of the silicon pits are modified by OTE which has low surface energy [40]. Polymer nanopyramid arrays can then be easily replicated by using the patterned silicon wafer as a reusable mold. The resulting nanopyramid arrays show striking iridescent colors and wafer-scale sample (as large as 4 inch) can be fabricated. Figure 3(A) shows the atomic force microscope (AFM) image of an array of ETPTA nanopyramids templated from the silicon pits as shown in figure 2. The ETPTA nanopyramid array clearly has retained the hexagonal ordering and the inter-pit distance of the silicon template. The nanopyramids have sharp tips and edges and most of the tips have radius of curvature of less than 5 nm. The inverted silicon molds can be reused multiple times before the

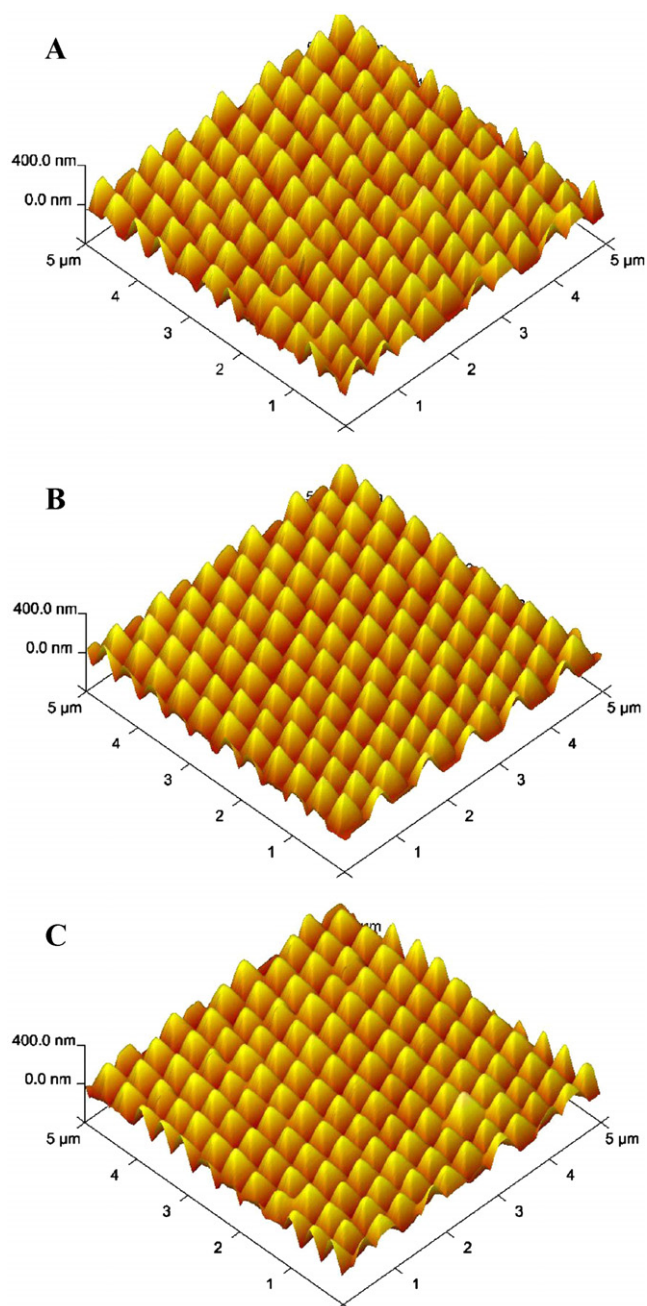


Figure 3. AFM images. (A) An array of polymer nanopyramids templated from the inverted silicon pyramidal pits as shown in figure 2. (B) The same polymer nanopyramid array coated with a 10 nm thick gold layer. (C) The same polymer nanopyramid array coated with a 50 nm thick gold layer.

OTE coating needs to be regenerated. A brief oxygen plasma etch followed by the OTE surface-modification process as discussed in the experimental section is sufficient to regenerate the silicon mold.

A thin layer of gold can finally be deposited on the surface of the templated polymer nanopyramid arrays by the conventional physical vapor deposition techniques (e.g., electron-beam deposition or sputtering) to finish the fabrication of SERS-active substrates. It is important that the thickness of the deposited gold determines the sharpness of the resulting

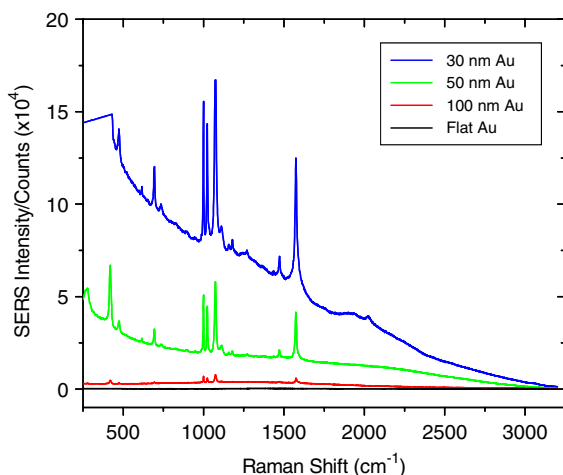


Figure 4. SER spectra obtained on a flat gold control sample and three polymer nanopyramid arrays coated with 30, 50, and 100 nm thick gold layers, respectively. The spectra were taken using a 785 nm diode laser at 4.8 mW with an integration time of 10 s.

nanopyramids. Figures 3(B) and (C) show the AFM images of the same ETPTA nanopyramid sample as shown in figure 3(A) covered with 10 and 50 nm thick gold, respectively. It is apparent that the nanotips of the 10 nm sample have the similar sharpness as those of the polymer nanopyramids, while the tips of the 50 nm sample are blunter than those of the polymer nanopyramids and the 10 nm sample. Although the conformal coverage of the polymer nanopyramids by the gold layer slightly compromises the sharpness of the inverted silicon pyramids, the much less amount of broken nanopyramids than the templated pure gold nanopyramids [32] compensates the potential loss of SERS enhancement.

To evaluate the SERS enhancement of the gold-covered polymer nanopyramids, we choose benzenethiol as a model molecule because of its ability to form self-assembled monolayers on gold surfaces and its large Raman cross-section. Figure 4 shows the SER spectra of the benzenethiol molecules adsorbed on a flat gold control sample and three arrays of polymer nanopyramids covered with 30, 50, and 100 nm thick gold layers, respectively. All three nanopyramid arrays display distinctive SERS peaks whose positions and relative amplitude agree well with those in the literature for benzenethiol molecules adsorbed on the structured gold surfaces [23, 42]. By contrast, the featureless gold control sample, which is prepared in the same sputtering batch as the nanopyramid arrays and thus should have the similar surface roughness, shows no clear SERS peaks. From the SER spectra, it is apparent that the 30 nm sample shows higher enhancement than the 50 and the 100 nm samples. The SERS enhancement factors for the three samples are estimated to be 1.2×10^8 , 5.0×10^7 , and 4.3×10^6 , respectively, by using the method described in the literature by comparing the Raman scattering intensity for the peak at 1080 cm^{-1} obtained for a solution and at the nanopyramid array and assuming a surface coverage of $0.45 \text{ nmol cm}^{-2}$ for benzenethiol on gold and the surface roughness of 3.0 [22, 23]. The high scattering background of the SER spectra, which defines the baseline for the Raman

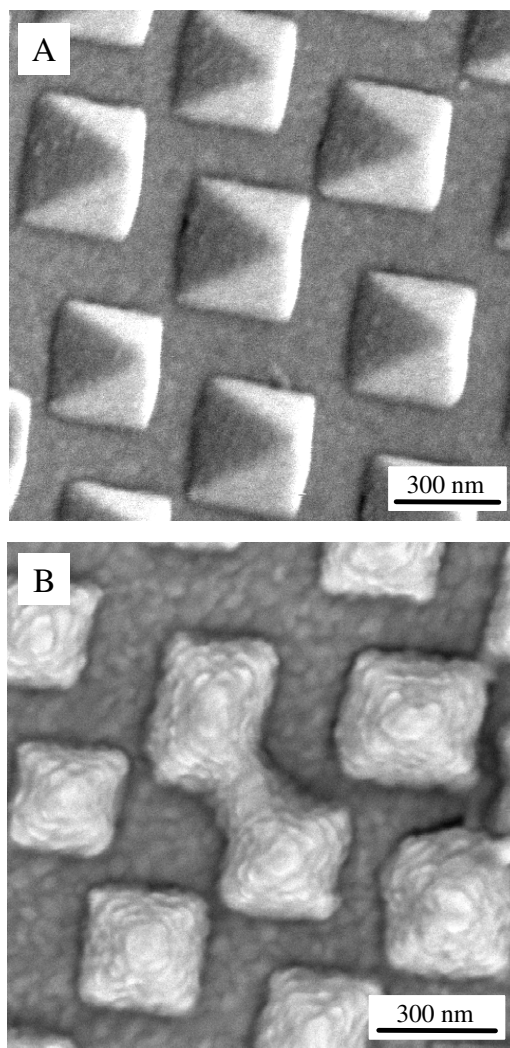


Figure 5. SEM images of the same polymer nanopyramid array coated with 30 nm (A) and 100 nm (B) thick gold layer.

signal, has been subtracted from the absolute counts to derive the Raman scattering intensity to calculate the resulting Raman enhancement factors. The 30 nm gold-covered nanopyramid array exhibits more than 2 orders of magnitude higher enhancement factor than that of the pure gold nanopyramids fabricated by our previous templating technique [32], where a 500 nm thick gold layer needs to be deposited to create the SERS substrate. The enhancement factor obtained for the gold-covered polymer nanopyramids compares favorably to those of periodic SERS substrates prepared by other colloidal templating approaches [23, 25], while almost 2 orders of magnitude larger sample can be fabricated by our current technique. In addition, the reusability of the silicon templates further improves the production throughput.

To help elucidate why the 100 nm gold-covered nanopyramid array exhibits much lower Raman enhancement than the 30 nm sample, we compare SEM images of these samples in figure 5. It is evident that the 100 nm Au nanotips are much rougher and blunter than the 30 nm nanotips, indicating the metal deposition process is far from ideal. Indeed, if ideal, conformal deposition occurs, we should

expect to obtain gold nanopylramids with similar roughness and sharpness for different gold thicknesses. We used sputtering to deposit gold on the polymer pyramids to make the SERS substrates. It is well known that sputtered metal films are usually rough. Metal clusters instead of individual atoms are generated and deposited by the bombardment of the metal target by high-energy ions. The accumulation of metal clusters makes the resulting nanotips rough and blunt, especially for thick deposition.

We speculate the electromagnetic enhancement caused by the strong concentration of the electromagnetic field in the vicinity of the sharp nanotips is the dominating mechanism for the observed high SERS enhancement at the gold-covered polymer nanopylramids. We conduct both experiments and theoretical simulations to verify this hypothesis. Experimentally, we put a flat poly(dimethylsiloxane) (PDMS) sheet on top of the gold-covered nanopylramids and then apply a force on the PDMS film to deform the tips of the nanopylramids. SEM images show the shape and the long-range hexagonal arrangement of the original nanopylramids do not change during the pressing process, only the sharp nanotips get flattened. Raman scattering measurements demonstrate that the enhancement factors of the deformed nanopylramids are at least 2–3 orders of magnitude lower than the original samples. Theoretically, we conduct finite-element electromagnetic modeling using the COMSOL Multi-physics software to calculate the electric field amplitude distribution and the corresponding Raman enhancement factors surrounding arrays of gold-covered polymer nanopylramids [37]. Since the periodic nanostructure is symmetric, we construct a simplified 2D model which can be considered as sections through a 3D nanopylramid array at the point of maximal enhancement (figure 6(A)). To numerically solve the 2D Maxwell's equations, 'perfect matched layers' (PML) and low-reflection boundary conditions are utilized for the simulation [38]. The widely used optical constants for gold [43] are used to conduct the electromagnetic modeling and the surrounding medium is air.

Figures 6(A) and (B) show the simulated distribution of SERS enhancement factor around two adjacent nanopylramids with base length of 320 nm, inter-pyramid distance of $\sqrt{2} \times 320$ nm, and nanotip radius of curvature of 1 and 5 nm, respectively. For both samples with different tip sharpness, the simulation results show that the significant enhancing of the electromagnetic field and the maximal SERS enhancement factors ($10^{5.1}$ and $10^{4.1}$) occur at the vertices of the nanotips. The localization of electromagnetic field is tighter for the 1 nm tips as the electromagnetic 'hot spots' occupy a smaller area than the blunter tips. The spatial distribution of the 'hot spots' around the two triangles for both samples is asymmetric. This is caused by the electromagnetic interaction between the neighboring nanotips. Figure 6(C) shows that the larger arrays with more nanotips result in higher enhancement and the maximal enhancement factor reaches a plateau when the array has more than 18 tips for both samples with radius of curvature of 1 and 5 nm. In the real SERS experiments, the laser spot (size $\sim 40 \mu\text{m}^2$) can cover ~ 250 nanopylramids. To evaluate the contribution of the tip sharpness to the SERS enhancement, we calculate the maximal enhancement factor (G_{max}) for six

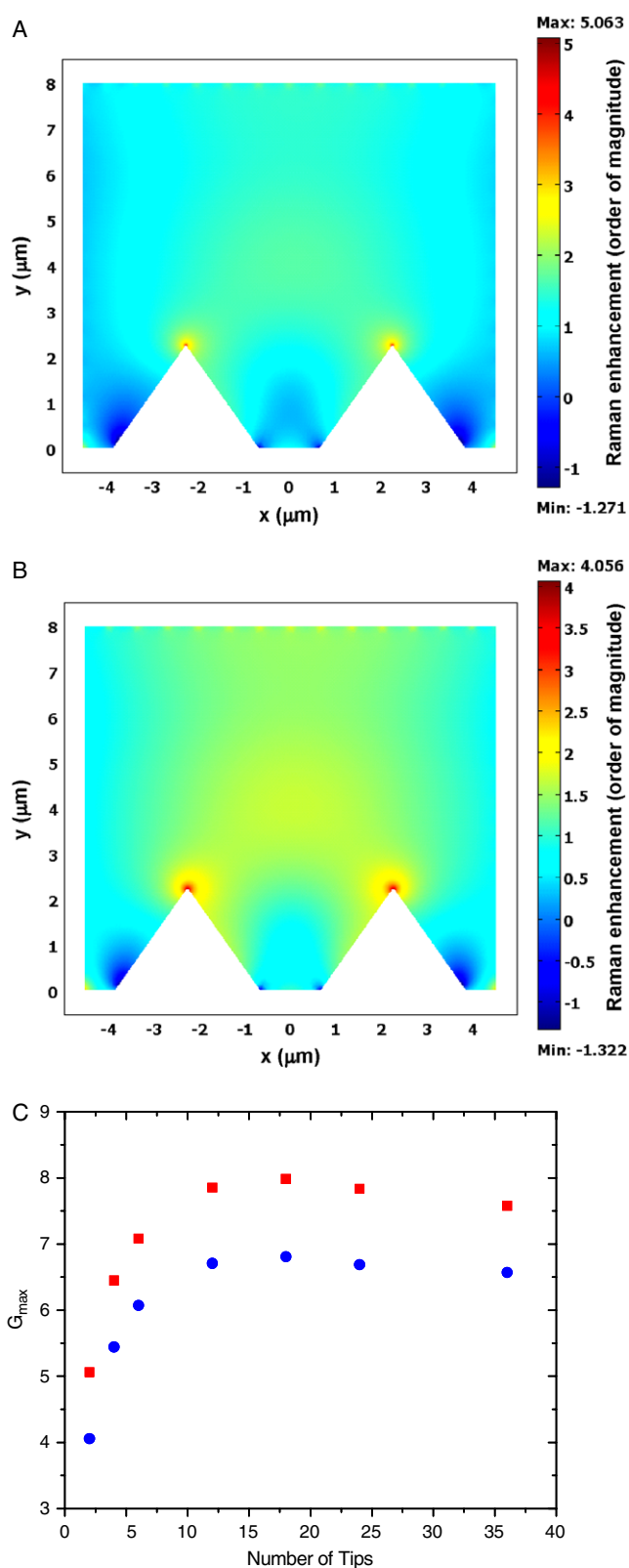


Figure 6. Simulated Raman enhancement factor around two gold-covered polymer nanopylramids with base length of 320 nm and tip radius of curvature of 1 nm (A) and 5 nm (B) at $\lambda = 785$ nm. (C) Simulated maximal SERS enhancement factor (G_{max}) versus number of tips of the gold-covered polymer nanopylramids with tip radius of curvature of 1 (red) and 5 nm (blue).

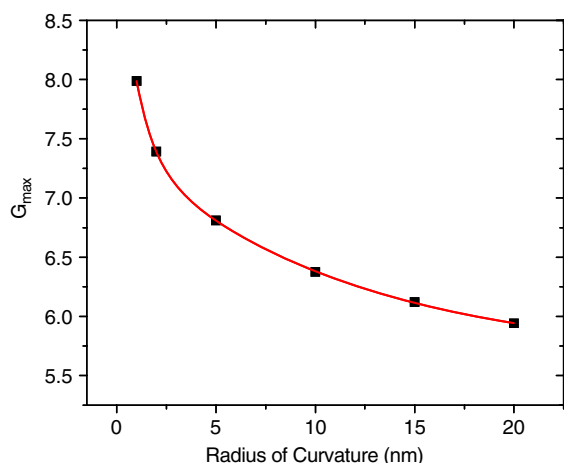


Figure 7. Simulated maximal SERS enhancement factor versus sharpness of templated nanotips for six nanopyramid samples with the same number of tips ($n = 18$) but different radius of curvature.

samples with the same number of tips ($n = 18$) but different sharpness (radius of curvature = 1, 2, 5, 10, 15, 20 nm). The simulated results are shown in figure 7. It is evident that more than 100-fold decrease in G_{\max} occurs when the sharpness of the nanotips is reduced by only 20-fold. This could explain the experimental results in figure 4 where thinner gold coating (i.e., sharper nanotips) leads to higher enhancement.

Although the simulated G_{\max} has the same order of magnitude ($\sim 10^8$) as the maximal enhancement factor obtained from experiment, several points need to be clarified. First, the current 2D simulation result underestimate the real value as the sharp edges and facets of the 3D nanopyramids are not being considered. Second, the effective area occupied by the electromagnetic ‘hot spots’ is quite small. If we calculate the enhancement of Raman scattering by averaging G_{\max} by weighting the effective area, the result will be much smaller than the simulated G_{\max} . Fortunately, a recent experimental study shows that a very small percentage of molecules (0.0063%) in the hottest spots contribute 24% to the overall SERS intensity [44]. Third, the charge transfer (CT) enhancement arising from the electronic interaction between the analytes at the metal surface [45] is not being considered by the current simulation model.

4. Conclusions

In conclusion, we have developed a non-lithographic technology for fabricating periodic arrays of gold-covered polymer nanopyramids with nanoscale sharp tips. The sharpness of the nanotips can be easily tuned by controlling the thickness of the deposited gold layer. These high-density arrays of nanotips can significantly enhance the local electromagnetic field at the tip apex, resulting in high SERS enhancement. Finite-element electromagnetic modeling further demonstrates the crucial role played by the sharp nanotips in determining the SERS enhancement factor. This new colloidal templating technique enables the large-scale fabrication of structured SERS substrates that are almost 2

orders of magnitude larger than those made by other bottom-up approaches and is promising for developing ultra-sensitive sensors for trace chemical and biological analysis.

Acknowledgments

This work was supported in part by the NSF under Grant No. CBET-0651780 and CBET-0744879, ACS Petroleum Research Fund, the start-up funds from the University of Florida, and the UF Research Opportunity Incentive Seed Fund.

References

- [1] Baker G A and Moore D S 2005 *Anal. Bioanal. Chem.* **382** 1751–70
- [2] Barnes W L, Dereux A and Ebbesen T W 2003 *Nature* **424** 824–30
- [3] Dieringer J A, McFarland A D, Shah N C, Stuart D A, Whitney A V, Yonzon C R, Young M A, Zhang X Y and Van Duyne R P 2006 *Faraday Discuss.* **132** 9–26
- [4] Haynes C L, Yonzon C R, Zhang X Y and Van Duyne R P 2005 *J. Raman Spectrosc.* **36** 471–84
- [5] Kneipp K, Kneipp H and Kneipp J 2006 *Acc. Chem. Res.* **39** 443–50
- [6] Murray W A and Barnes W L 2007 *Adv. Mater.* **19** 3771–82
- [7] Ozbay E 2006 *Science* **311** 189–93
- [8] Stewart M E, Anderton C R, Thompson L B, Maria J, Gray S K, Rogers J A and Nuzzo R G 2008 *Chem. Rev.* **108** 494–521
- [9] Tian Z Q, Ren B and Wu D Y 2002 *J. Phys. Chem. B* **106** 9463–83
- [10] Zhang X Y, Young M A, Lyandres O and Van Duyne R P 2005 *J. Am. Chem. Soc.* **127** 4484–9
- [11] Kelf T A, Sugawara Y, Cole R M, Baumberg J J, Abdelsalam M E, Cintra S, Mahajan S, Russell A E and Bartlett P N 2006 *Phys. Rev. B* **74** 245415
- [12] Sugawara Y, Kelf T A, Baumberg J J, Abdelsalam M E and Bartlett P N 2006 *Phys. Rev. Lett.* **97** 266808
- [13] Nie S M and Emery S R 1997 *Science* **275** 1102–6
- [14] Qian X M and Nie S M 2008 *Chem. Soc. Rev.* **37** 912–20
- [15] Braun G, Pavel I, Morrill A R, Seferos D S, Bazan G C, Reich N O and Moskovits M 2007 *J. Am. Chem. Soc.* **129** 7760–1
- [16] Freeman R G *et al* 1995 *Science* **267** 1629–32
- [17] Wang H, Levin C S and Halas N J 2005 *J. Am. Chem. Soc.* **127** 14992–3
- [18] Jackson J B and Halas N J 2004 *Proc. Natl Acad. Sci. USA* **101** 17930–5
- [19] Roca M and Haes A J 2008 *J. Am. Chem. Soc.* **130** 14273–9
- [20] Jeanmaire D L and Van Duyne R P 1977 *J. Electroanal. Chem.* **84** 1–20
- [21] McLellan J M, Li Z Y, Siekkinen A R and Xia Y N 2007 *Nano Lett.* **7** 1013–7
- [22] Abdelsalam M E, Mahajan S, Bartlett P N, Baumberg J J and Russell A E 2007 *J. Am. Chem. Soc.* **129** 7399–406
- [23] Cintra S, Abdelsalam M E, Bartlett P N, Baumberg J J, Kelf T A, Sugawara Y and Russell A E 2006 *Faraday Discuss.* **132** 191–9
- [24] Dick L A, McFarland A D, Haynes C L and Van Duyne R P 2002 *J. Phys. Chem. B* **106** 853–60
- [25] Haynes C L and Van Duyne R P 2001 *J. Phys. Chem. B* **105** 5599–611
- [26] Tessier P M, Velev O D, Kalambur A T, Rabolt J F, Lenhoff A M and Kaler E W 2000 *J. Am. Chem. Soc.* **122** 9554–5

- [27] Henzie J, Barton J E, Stender C L and Odom T W 2006 *Acc. Chem. Res.* **39** 249–57
- [28] Kahl M, Voges E, Kostrewa S, Viets C and Hill W 1998 *Sensors Actuators A* **51** 285–91
- [29] Kosiorek A, Kandulski W, Chudzinski P, Kempa K and Giersig M 2004 *Nano Lett.* **4** 1359–63
- [30] Lu Y, Liu G L, Kim J, Mejia Y X and Lee L P 2005 *Nano Lett.* **5** 119–24
- [31] Liu G L, Lu Y, Kim J, Doll J C and Lee L P 2005 *Adv. Mater.* **17** 2683
- [32] Sun C H, Linn N C and Jiang P 2007 *Chem. Mater.* **19** 4551–6
- [33] Lin T H, Linn N C, Tarajano L, Jiang B and Jiang P 2009 *J. Phys. Chem. C* **113** 1367–72
- [34] Stober W, Fink A and Bohn E 1968 *J. Colloid Interface Sci.* **26** 62
- [35] Jiang P and McFarland M J 2004 *J. Am. Chem. Soc.* **126** 13778–86
- [36] Jiang P, Prasad T, McFarland M J and Colvin V L 2006 *Appl. Phys. Lett.* **89** 011908
- [37] Brown R J C, Wang J, Tantra R, Yardley R E and Milton M J T 2006 *Faraday Discuss.* **132** 201–13
- [38] Jin J 2002 *The Finite Element Method in Electromagnetics* (New York: Wiley)
- [39] Moskovits M 1985 *Rev. Mod. Phys.* **57** 783–826
- [40] Peanasky J, Schneider H M, Granick S and Kessel C R 1995 *Langmuir* **11** 953–62
- [41] Madou M J 2002 *Fundamentals of Microfabrication: The Science of Miniaturization* (Boca Raton, FL: CRC Press)
- [42] Guieu V, Lagugne-Labarthe F, Servant L, Talaga D and Sojic N 2008 *Small* **4** 96–9
- [43] Johnson P B and Christy R W 1972 *Phys. Rev. B* **6** 4370–9
- [44] Fang Y, Seong N H and Dlott D D 2008 *Science* **321** 388–92
- [45] Campion A, Ivanecy J E, Child C M and Foster M 1995 *J. Am. Chem. Soc.* **117** 11807–8